Effect of Chain Entanglements on Plastic Deformation Behavior of Linear Polyethylene

Z. Bartczak†

Centre of Molecular Macromolecular Studies, Polish Academy of Sciences, Sienkiewicza 112, 90-363 Lodz, Poland

Received April 18, 2005; Revised Manuscript Received July 7, 2005

ABSTRACT: Samples of semicrystalline polyethylene in which the chain topology within the amorphous component was altered by using two-stage processing, including crystallization in a chain-extended fashion at high pressure in the first step, were produced, and their deformation behavior in the plane-strain compression was studied. The deformation and recovery experiments evidenced that the state of the molecular network governed by entanglements density is one of the key parameters controlling the response of the material on imposed strain, especially in the range of moderate and high strains. It influences markedly the shape of the true stress−true strain curve, changing the strain hardening modulus and the onset of strong strain hardening. The strain hardening modulus decreases while onset of strong strain hardening increases with a decrease of the entanglement density within amorphous component. Depending on the density of entanglements, PE samples demonstrated various amount of rubberlike recoverable deformation and permanent plastic flow. In the case of reduced concentration of entanglements the permanent flow was easier than in materials with higher entanglement density and could set in quite early, at relatively low strains, becoming a favorable deformation mechanism. As a result, the strong strain hardening was postponed to higher strains as compared to samples of equilibrium entanglement density. When the topology of amorphous component was modified to increase the network density, that network became stiffer with reduced ability of strain-induced disentangling of chains. Consequently, there was relatively less permanent flow and strain hardening begun earlier than in the reference material of unaltered chain topology.

1. Introduction

Entanglements between macromolecular chains are one of the basic implications of their considerable length and flexibility. Their existence has profound consequences on most of polymer properties in both liquid and solid states. The mutual interpenetration and numerous entanglements of macromolecules determines the course of many processes in which substantial fragments of chains are involved. Some of the most significant examples are flow of a melt, crystallization, and mechanical deformation of a solid polymer. However, despite numerous research, the role of chain entanglements and their impact on polymer properties is still not fully understood.

For the purpose of this report we can focus on the influence of topological structure of polymer, including entanglements between chains, on deformation of a solid semicrystalline polymer. Chain segments trapped between entanglements constitute the continuous network within amorphous component. The entanglements act then like cross-links. It is already well understood that orientation strain hardening in amorphous polymers originates from that topological structure.[1−3] This view is supported by the fact that strain hardening can be accurately described by a neo-Hookean relation.[3−6] The network properties of entangled chains influence also remarkably the deformation behavior of semicrystalline polymers. Crystallization proceeding at usual conditions does not remove chain entanglements preexisting in the melt. Although some are resolved by reeling in to the growing crystals, most of them is merely shifted into amorphous interlamellar regions.[7] This means redistribution usually on the length scale of about 10 nm, but globally, the isotropic entangled network of the melt is retained. That network should manifest by high reversibility of the deformation, which in fact is frequently noticed. The common observation is that drawn samples demonstrate an almost complete retraction to their original length when heated to the melting point.[8] Dramatically different strain hardening observed in melt- and solution-crystallized polyethylene of ultrahigh molecular weight samples, demonstrating different density of chain entanglements, also strongly suggest that entanglements play a major role in deformation of semicrystalline polymers.[9−11] Strobl et al.[12−17] focused on this aspect of the deformation of semicrystalline polymers which are related to the presence of molecular network. They found that network properties influence profoundly the deformation behavior of semicrystalline polymers. In a recent study of deformation of polyethylene the direct correlation between molecular weight, controlling the number of entanglements in a solid polymer, and the strain hardening behavior was found.[18]

Entangling of chains is a spontaneous process and therefore is difficult to control. However, in the case of semicrystalline polymer the number of entanglements persisting in the amorphous phase after crystallization actually depends on the conditions of crystallization process and therefore can be modified in a certain limited range. For example, the density of entanglements can be considerably reduced in samples crystallized from dilute solution[9−11] or in samples of relatively low molecular weight crystallized slowly from the melt.[19] Another possibility offers crystallization during polymerization.[20] Crystallization in chain-extended fashion under elevated pressure also allows for a substantial decrease of the number of entanglements at appropriate

† Tel +48 (42) 681.89.52, e-mail bartczak@bilbo.cbmm.lodz.pl.

10.1021/ma050815y CCC: $30.25
Published on Web 08/13/2005

Table 1. Characteristic of Polymers Studied

sample code	manufacturer	M_w	polydispersity	MFI[a] (g/10 min)	density[b] (g/cm^3)
PE-1	Millennium Petrochemicals (Cincinnati, OH)	0.57×10^5	3.5	6.7	0.957
PE-2	BASF	1.2×10^5	3.4	2.3	0.943

[a] 190 °C, 2.16 kG (ASTM D-1238). [b] Quenched samples.

crystallization conditions.[21] Unfortunately, in every of these approaches the modification of the molecular network is always accompanied by a profound modification of the crystalline structure, which seriously limits the use of any of them to study the influence of the molecular network on deformation behavior.

Psarski et al.[22] proposed recently a new method of preparation of samples of polyethylene with reduced concentration of entanglements, while nearly unaltered crystalline structure as compared to the initial material. The idea of this approach based on differences of melting of chain-folded and chain-extended polyethylene crystals. Melting of disentangled chain-folded PE crystals (e.g., obtained by crystallization from dilute solution) leads to immediate reentangling.[9−11] Consequently, the solution crystallized disentangled sample can be drawn to very high strain with practically no strain hardening, while the same sample subjected to even very short-time melting followed by crystallization demonstrates the strain hardening behavior typical for a virgin, not manipulated material.[9−11] That effect of immediate reentangling is most probably due to chain folds. There are arguments supported by experimental observations[23] that chain-folded crystals "explode" upon melting, and the fold energy is released in an sudden, springwise manner. The molecule in the crystal is like a coiled spring constrained from expanding by the lattice forces. Once these constraints are removed by melting, the chains spring out rapidly, driven by the need to increase its entropy. Chain segments are then ejected with a high kinetic energy into the already molten surrounding and interlace with other chains rapidly.

A quite different melting behavior can be expected for chain-extended crystals, in which the basal planes consist mainly of chain ends instead of folds. Such a crystal plane does not require relaxing of its energy on melting, and chains are not supposed to be translocated to a large extent. The basic conformational change is then the entropy-driven coiling. Therefore, melting of such crystals does not increase significantly the number of entanglements over that already resident in the amorphous phase prior to melting. Furthermore, if the amorphous phase contains very few entanglements and/or the degree of crystallinity is very high, which is common in samples containing chain-extended crystals, melting should lead to the topological structure with the average distance between entanglement knots M_e close to M. That disentangled state should persist in the melt for a period of time, which is needed for a macromolecule to reptate to the entirely new position. The chains in an initially disentangled melt are subject of thermally activated segmental diffusion. As the chains diffuse between each other, the entanglements are gradually restored up to the point of equilibrium concentration. That reentangling process can be imagined as a creation of a reptation tube for each chain. The time needed may be roughly estimated from approximately $\tau_r \sim 10^3$ s for linear PE of $M_w \sim 5 \times 10^4$ [22] to much more than 10^4 s for UHMWPE of $M_w \sim 10^6$.[24] The process of restoration of the entanglement network can be interrupted at any point by rapid quenching of the melt. This "freezes" also the number of entanglements in the material since fast crystallization does not change the overall number of entanglements in the material and only redistributes them in the scale length of few nanometers, as mentioned earlier. Therefore, it appeared possible to obtain a series of samples of polyethylene of various topological structure, characterized by the number of entanglements, by differentiation of the residence time in the melt of the initially chain-extended crystalline sample, followed by fast crystallization. That approach was tested successfully by Psarski et al.[22] in the study of the influence of entanglements on crystallization.

The method used to obtain samples consisting of chain extended crystals, necessary to obtain disentangled melt, based on the existence of the region of pseudohexagonal phase on the phase diagram of polyethylene in which the formation of significantly thicker crystals is possible. As reported by many authors (e.g., refs 25 and 26), the crystallinity degree of PE samples crystallized under high pressure can reach 99% while the crystal thickness can exceed the length of fully extended polymer chains. Crystals as thick as 3 μm were obtained by Geil et al.,[27] which indicates that more than a single extended chain can be incorporated within the crystal thickness. It was also shown that chain-extended crystals can be formed not only by crystallization from the melt but also on high-pressure annealing of chain-folded crystals, close to the melting temperature.[28,29] Orthorhombic PE crystals are transformed at the pressure above 300 MPa to pseudohexagonal form,[30] and their thickness increases,[31] even to several micrometers.[32] This thickening is accompanied by dramatic increase of overall crystallinity.[33]

The goal of the presented study was to investigate an influence of the entanglements on the deformation of polyethylene, including the strain hardening behavior at high strain. To accomplish that, we decided to prepare samples of polyethylene of various concentration of entanglements according to the method outlined above. As a deformation mode the plane-strain compression was chosen. This mode allows for homogeneous, stable, and cavity-free deformation in a broad strain range. Moreover, the true stress−true strain curves, characterizing the deformation process, can be obtained easily in this deformation mode.

2. Experimental Section

2.1. Materials and Sample Preparation. Two commercial grade samples of linear polyethylene well stabilized against thermal degradation were used in this study. Their molecular characteristics are summarized in Table 1.

Cylindrical samples for high-pressure crystallization were prepared from both PE-1 and PE-2 polyethylenes by injection molding. They were loaded into a pressure cell consisting of a barrel of 9.5 mm inner diameter, made of ultrahigh strength steel, and two matching tungsten carbide pistons. The copper seals placed between sample and the pistons prevented any leakage of the polymer out of the cell. The pressure was applied to the cell by compression in a computer-controlled 50 kN loading frame of the tensile testing machine (Instron 1114). The hydrostatic pressure inside the cell was controlled with

an accuracy of ±0.2 MPa. Other details of the experimental setup were given elsewhere.[22,33]

The high-pressure transformation of samples was performed by annealing at an elevated temperature under high pressure. The temperature of 244−245 °C and hydrostatic pressure of 480 MPa were used throughout this study. At such conditions orthorhombic crystals of PE are transformed to the pseudohexagonal phase of high mobility. Annealing allows for substantial thickening of chain-folded crystals, leading to the formation of chain-extended ones. Most of preexisting chain entanglements is resolved, resulting in substantial increase of crystallinity.[33] After a 30 min−1 h time period of high-pressure annealing the cell was cooled to room temperature, and then pressure was released. On cooling, the chain-extended hexagonal crystals transformed back to the orthorhombic phase, yet their chain-extended morphology and low concentration of chain entanglements were preserved.

From the high-pressure crystallized PE billets the samples for further mechanical studies were prepared. From every billet, ∼22 mm long, a 4 mm thick slice was machined out for further studies of the properties of high-pressure material. The remaining piece was divided into two parts, which were subjected to remelting and subsequent fast crystallization. To do that, specimens were put into the cylindrical mold (12 mm i.d., 4.5 mm in height). The mold was placed in a laboratory press heated to the temperature of 160 °C to melt a polymer inside. After defined residence time from the range between 3.5 and 32.5 min, the mold was quickly transferred from the press into the bath of ice−water to induce fast crystallization of polymer inside. It was determined that the time needed for melting the sample and reaching the annealing temperature was ∼2.5 min. Therefore, the effective time of melt-annealing varied from 1 to 30 min. Solidified disks of PE were machined into the form of rectangular prisms 4 mm high and 6 mm wide, subsequently used in plane-strain compression experiments. During machining the specimen and the tool were continuously cooled to prevent any unwanted structural changes due to local heating.

2.2. Thermal Analysis and Density. The thermal analysis of the samples was conducted using a TA 2920 DSC apparatus (TA Instruments). Melting thermograms were recorded at the heating rate of 10 °C/min, under nitrogen flow. The crystallinity was estimated from the heat of melting (the value of $\Delta h_f = 293$ J/cm^3,[34] for 100% crystalline PE was used).

The crystallinity of the specimens was evaluated independently also from the density determined by the flotation method. Densities of crystalline and amorphous phase of 1.0 and 0.855 g/cm^3, respectively, were used for calculation of the crystallinity.

2.3. Microscopy. For evaluation of the morphology of the original and processed samples the specimens were first prepared by cutting with an ultramicrotome in order to expose a flat and smooth cross-section surface. That surface was etched with permanganic etchant mixture according to the procedure developed by Olley et al.[35] Etching by ∼1 h at room temperature was usually adequate to reveal crystalline morphology of the sample on the exposed surface. Etched specimens coated with fine layer of gold were examined with a scanning electron microscope (JEOL JSM 5500LV). Additionally, the nonetched fracture surfaces of respective samples were also inspected.

2.4. Dynamic Mechanical Properties. Dynamic mechanical properties of selected samples were probed in the bending mode with the DMTA apparatus (Mk III, Rheometric Sci.) at a frequency of 1 Hz and a heating rate of 2 °C/min.

2.5. Mechanical Testing. Rectangular specimens prepared according to the procedure described in section 2.1 were tested in the plane-strain compression at room temperature. The plane-strain compression tests were performed using an universal tensile testing machine (Instron 5582) equipped with a special compression accessory of the type of channel die, described elsewhere.[18] The samples 6 mm wide, 4 mm high, and 5 mm long were placed in the die and compressed with a constant speed of the crosshead at room temperature. The crosshead speed of 0.2 mm/min provided the initial deformation rate of 8.3×10^{-4} s^{-1}.

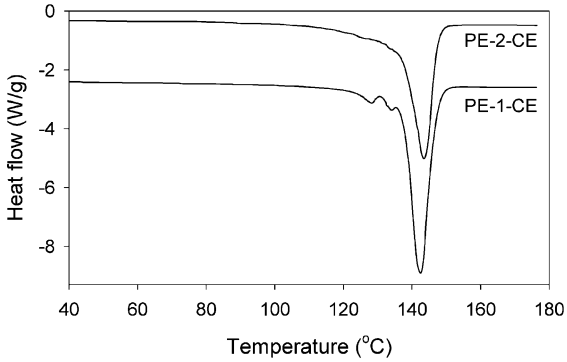

Figure 1. Representative DSC melting curves of high-pressure crystallized samples. The heating rate was 10 °C/min. Curves were shifted along heat flow axis for clarity of presentation.

Since in a channel-die geometry the cross section of the deformed sample under load stays constant, equal to the area of the plunger, the force measured by the loading cell could be simply transformed to the true stress. To determine the strain, a precise extensometer was attached to the die, very close to the sample. From the collected displacement data, corrected for compliance of the die, the true strain was calculated as $e = \ln(\lambda)$, where $\lambda = CR = h_0/h$ is the compression ratio. On the basis of these data, the true stress−true strain curves were constructed.

In a separate compression experiment the strain recovery behavior was studied. The experiment arranged for this implemented a step-and-cycle loading program:[12,18] the specimen was deformed first to some preselected strain, and then the crosshead was stopped and immediately retracted until load reached back zero. At this point the direction of the crosshead was reverted again, and the sample was compressed, now to another strain, higher than that reached in a previous cycle. Next, the specimen was unloaded once more and the cycle repeated. In such a stepwise manner the specimens were deformed up to the high strains, comparable to those reached for the same material in continuous loading experiment.

3. Results and Discussion

3.1. High-Pressure Crystallization. Samples of polyethylenes under study were crystallized at high pressure conditions in order to transform the crystals into chain-extended form (CE) and consequently highly reduce or possibly eliminate chain entanglements. Figure 1 presents DSC melting curves of high-pressure transformed samples. Both PE-1-CE and PE-2-CE exhibited a sharp melting peak centered around 143−144 °C, frequently accompanied by two small secondary peaks on its low-temperature shoulder. The main peak represents the melting of these thick crystals which were formed during high-pressure stage in hexagonal form and transformed on cooling into orthorhombic crystals. The additional peaks represent melting of thinner crystals formed probably in a secondary process, during cooling the sample down. Table 2 summarizes the temperatures of the primary melting peak and the degree of crystallinity, determined independently from DSC and density data. It must be noted here that the melting temperature determined by DSC may be overestimated due to overheating effects. Thus, any estimation of lamellar thickness from these data could be quite inaccurate. Therefore, the thickness of lamellae was determined from direct microscopic observations.

Figure 2a shows a representative SEM micrograph of etched surface of PE-1 sample. The thickness of the

Table 2. Thermal Properties of High-Pressure Crystallized Samples

sample	T_m[a] (°C)	X_c[a] (wt %)	X_c[b] (wt %)	av lamellae thickness, l[c] (nm)
PE-1-CE	142.4−143.0	99.5−100	100	600
PE-2-CE	143.1−144.3 (max = 144.9)	89.3−93.0	92−93.5	300

[a] Range of typical values observed for various samples, determined from DSC data. [b] Determined from density measurements. [c] Estimated from SEM micrographs.

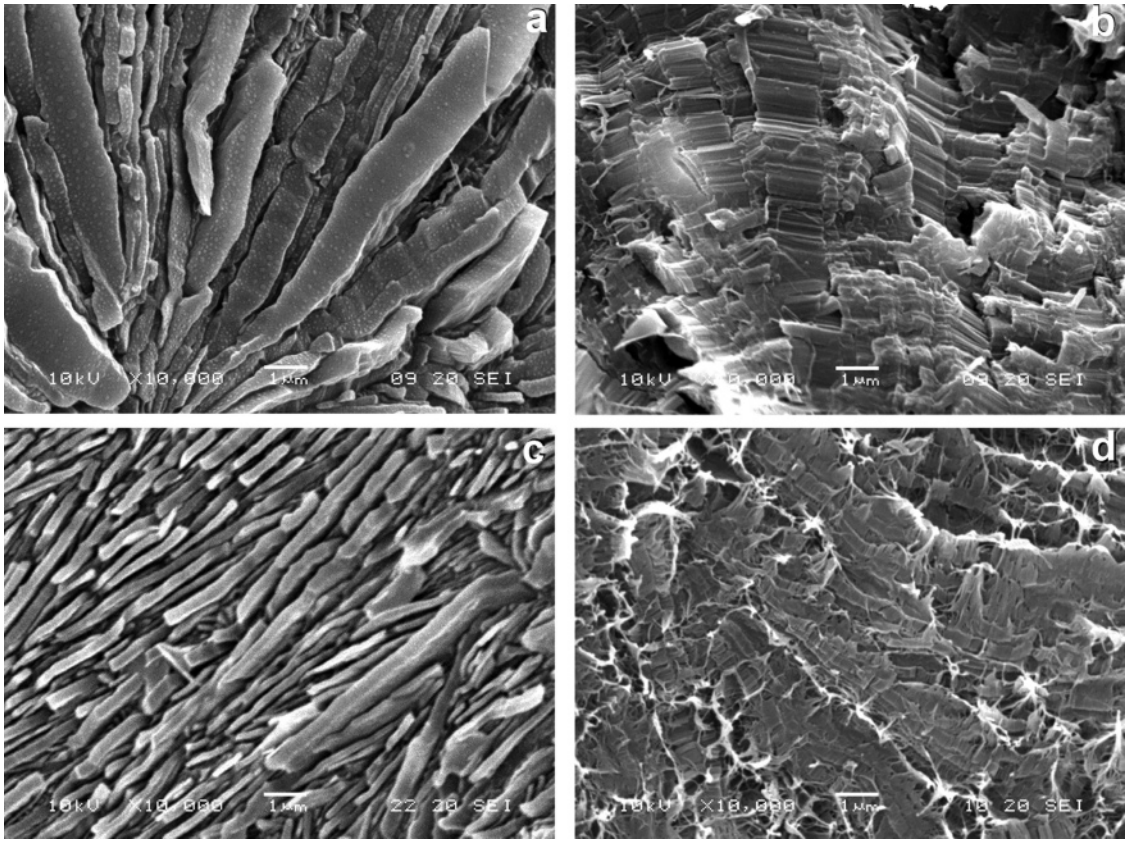

Figure 2. Scanning electron micrographs of high-pressure crystallized samples: (a) PE-1-CE cut and etched surface, (b) PE-1-CE fracture surface, (c) PE-2-CE cut and etched, (d) PE-2-CE fracture. Distance marker shown on each micrograph.

observed lamellae varied from 150 nm up to more than 1 μm, with the average of ~600 nm. Crystal thickness, observed in SEM, considerably larger than the average chain length (l_{max} = 150 nm, as estimated from M_n), strongly supports extended conformation of chains within crystals. Moreover, for many thick crystals more than one extended chain was necessary to fill its thickness. Finally, the crystallinity observed in these samples was nearly 100% (cf. Table 2), which means that in absence of the amorphous phase the PE-1-CE chain-extended sample was practically free of any chain entanglements. The absence of the amorphous phase can be confirmed by examination of micrographs of etched and fractured surfaces of PE-1-CE, presented in parts a and b of Figure 2, respectively. Both micrographs show dense packing of lamellae. If the amorphous phase was present in the sample, the etched surface should contain deep grooves between lamellae (left by etched out interlamellar amorphous material), while on the fracture surface some traces of plastically deformed amorphous material could be expected. However, the micrographs do not show any of these features: lamellae tightly adjoin each other, while the fracture surface is clean, without any mark of plastic deformation, which clearly confirms an absence of any amorphous component.

The lamellae thickness in high-pressure crystallized specimens of PE-2 was within the range 80−400 nm, with the average thickness around 300 nm (representative SEM micrographs of fractured and etched surfaces shown in parts c and d of Figure 2, respectively). Assuming the tilt angle of the chain within lamella of 34.5°,[36] the average thickness of 300 nm corresponds to the average length of crystalline stem of about l^* = 360 nm, which is again above the estimated average length of fully extended chain in PE-2, l_{max} = 320 nm. This proves that also in sample PE-2-CE the crystals produced by high-pressure annealing consisted mostly of chains in the extended conformation. The crystallinity of PE-2-CE specimens was around 93 wt %. This shows that not all of material was able to crystallize in the high-pressure regime, probably due to entanglements of the longest chains, present in the initial sample. These entanglements could not be completely resolved during the transformation of chain-folded crystals into chain-extended form due to strong constraints and time limitations. The presence of a small fraction of the amorphous component can be also deduced from the micrographs presented in Figure 2. Micrograph of etched surface (Figure 2c) reveals thin gaps between lamellae, created due to preferred etching of amorphous layers. On the other hand, the nonetched fracture surface (Figure 2d) demonstrates thin linear zones of ductile fracture located between lamellae, which can be attributed to the plastic deformation of these amorphous layers.

3.2. Modification of Density of Chain Entanglements. From the chain-extended and disentangled samples described above the samples with expected various entanglement density were prepared by melt-annealing at $T = 160$ °C, followed by fast crystallization (quenching). Samples annealed for $t = 1$, 3, 10, 20, and 30 min were made. The reference samples obtained from PE-1 and PE-2 containing initially the ordinary chain-folded crystals were also prepared in a similar way.

At the moment of melting and shortly after, the samples of PE-1 and PE-2 consisted of nearly completely disentangled melt (as discussed above PE-1 was believed to be entanglement free, while for PE-2 the expected average entanglement was extremely low). Such a topological structure can persist in a melt for a relative short time. Then, because of thermally stimulated segmental diffusion of chains, the entanglements should be gradually restored. The time necessary for complete reentangling of chains may be roughly estimated on the basis of reptation theory as $\tau_r \sim 1.2 \times 10^3$ s for PE-1[22] and about twice longer for PE-2. Therefore, the concentration of entanglements present in the melt was anticipated to increase with increasing time of melt-annealing from an initial very low value up to the equilibrium value, characterized by the average molecular weight of the segment between entanglements of $M_e = 1240$,[37,38] all occurring within the time interval of τ_r, dependent on molecular weight of a polymer (i.e., 20−40 min for polymers studied here). Quenching of such a melt undergoing reentangling process at any given time lapsed should result in "freezing" of the entanglement density reached by the melt until this point due to fast crystallization in the chain-folded fashion. Since the conditions of the crystallization were always the same, the samples of a given polyethylene annealed at various times were expected to exhibit very similar properties of crystalline phase (crystal sizes, crystallinity, etc.), yet substantially different properties of the amorphous component due to different concentration of entanglements. The properties of the network of entanglements belong to those principal parameters which determine the response of semicrystalline polymer on mechanical deformation, especially at large strains.[12]

The specimens melt-annealed for 1 min, labeled PE-1-1 and PE-2-1, had presumably low concentration of entanglements in the amorphous component, as considered above, while PE-1-30 and PE-2-30; i.e., those annealed for 30 min were expected to exhibit the concentration of entanglements close to the equilibrium. Samples annealed for 3, 10, and 20 were expected to show an intermediate entanglement densities. It should be noted that because for every case the respective PE-n-CE, PE-n-1 and PE-n-30 ($n = 1$ or 2) specimens were prepared from the same billet of chain-extended and disentangled material, they had identical starting chain topology, which was subsequently differentiated by variation of the annealing conditions. DSC melting studies demonstrated that after such a thermal treatment specimens of a given polymer exhibited very similar properties of crystalline phase, with melting temperature varying less than 0.5 °C and degree of crystallinity varying less than 2 wt % as well as similar spherulitic morphology within a set consisting the pair of melt-annealed samples and the respective reference sample prepared from virgin polymer at the same conditions of crystallization. The average values of T_m and X_c were 132.4 °C and 71.6 wt % for PE-1 while 130.6 °C and 64 wt % for PE-2, respectively. DSC curves presented in Figure 3 illustrate the discussed features.

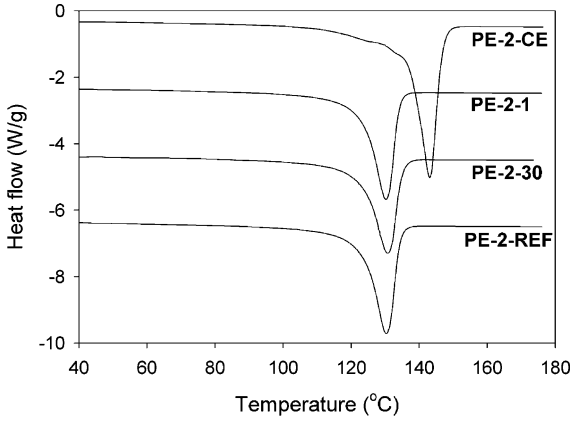

Figure 3. DSC melting curves of samples obtained from PE-2 polymer: high-pressure PE-2-CE (upper curve), the same after melt-annealing by 1 min at 160 °C followed by quenching, PE-2-1 (middle), and after melt-annealing by 30 min at 160 °C followed by quenching, PE-2-30 (bottom curve). The heating rate was 10 °C/min. Curves were shifted along heat flow axis for clarity.

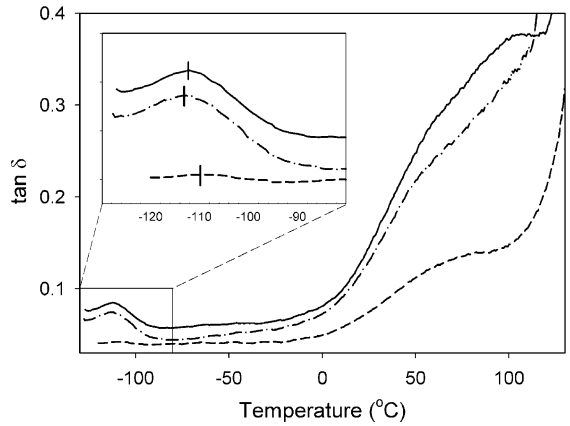

Figure 4. Loss tangent curves of samples of PE-2 measured by DMTA: PE-2-REF (solid line), PE-2-CE (dashed line), and PE-2-1 (dash−dotted line). Curves were shifted vertically for clarity of presentation. Inset shows enlarged portion of the curves in the range of γ relaxation.

The dynamical mechanical behavior was probed with DMTA. Figure 4 presents the plot of tan δ of selected samples of PE-2. In absence of the β-relaxation peak, which is common for linear polyethylenes, only the range of γ relaxation may provide some, although limited, information about constitution of the amorphous component. This relaxation is related to the mobility of short chain sequences in amorphous phase ("crankshaft mechanism").[39] While the variation of intensity of the γ peak reflects simply different amount of the amorphous phase, the changes of its position, marked in Figure 4, may suggest a reduced mobility of chain segments in the PE-2-CE sample and a slightly increased one in PE-2-1 as compared to the PE-2-REF. The PE-2-30 sample (curve not presented) shows γ relaxation practically identical to that of the reference. Such a behavior seems to be consistent with the anticipated differences of the entanglement density among discussed samples.

3.3. Stress−Strain Behavior. For both polymers the chain-extended and disentangled sample (PE-n-CE; $n = 1$, 2), chain-folded of presumably low, intermediate, and high entanglements density (PE-n-t; $t = 1$, 3, 10,

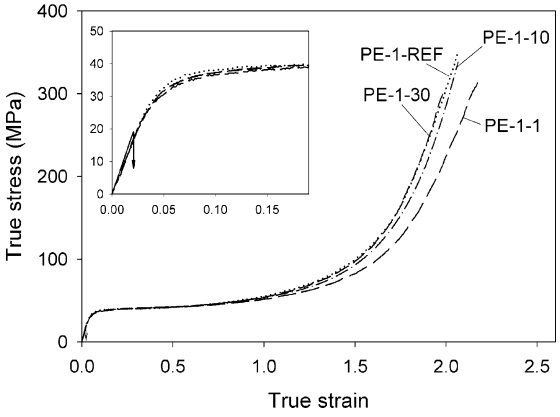

Figure 5. True stress-true strain curves of the samples of PE-1 polyethylene. Inset shows enlarged initial part of the same curves.

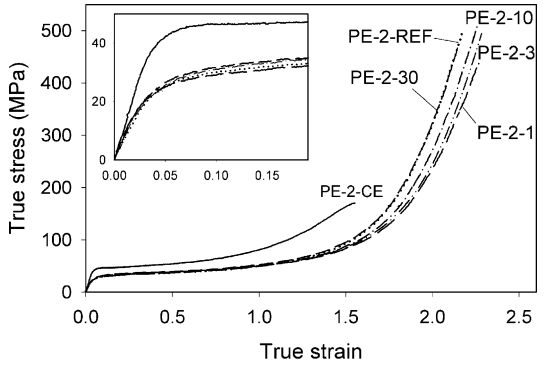

Figure 6. True stress-true strain curves of the samples of PE-2 polyethylene. Inset shows enlarged initial part of the same curves.

20, 30), as well as the reference sample (PE-*n*-REF) were deformed in plane-strain compression at room temperature. Figure 5 presents a set of true stress−true strain curves determined for the specimens of PE-1 polyethylene. The curves obtained for PE-1-3 specimens demonstrated the shape very close to that of PE-1-1, while those obtained for PE-1-20 were practically identical with the curves obtained for PE-1-30 and the reference sample PE-1-REF. Therefore, for clarity of presentation these curves were not shown.

Specimens containing chain-extended crystals PE-1-CE (solid line) appeared extremely fragile and fractured before reaching the yield point, at the stress below 20 MPa. The elastic modulus was higher than found in the reference sample. Such a behavior reflects the structure of this sample: 100% crystalline, yet with no connectivity between thick crystals formed by completely extended chains. An opposite behavior was demonstrated by the reference sample PE-1-REF, consisting of chain-folded crystals separated by amorphous layers, which provide connectivity of crystallites through tie molecules and entanglement network. The density of entanglements in the amorphous phase and the number of tie-molecules connecting neighboring crystals in PE-1-REF are typical for melt-crystallized polyethylene. The reference material could be compressed at applied deformation conditions (i.e., geometry, strain rate, and temperature) to the true strain well above $e = 2.0$ ($CR > 7$). After yielding below $e = 0.1$, followed by plastic flow, the strain hardening stage set in at the true strain above ~0.6. This strain hardening in plane-strain compression leads to the very high stress of 470 MPa at the true strain of $e = 2.16$.[18] Extensive studies (see e.g. reviews[40−42]) demonstrated that such a stress response is a result of simultaneous deformation of crystalline component by crystallographic slip mechanisms and shear of amorphous layers, leading to strong orientation hardening. Both components are intimately connected and must deform simultaneously. Although the strain accommodated by crystallites is large, their deformation will be not discussed here in detail since practically all samples studied had nearly identical crystalline component (including amount, size, and any other properties of crystallites), so that deformation of crystalline component was expected to proceed in very similar fashion and give nearly identical contribution to the overall strain in all samples. The samples produced from initially disentangled melt, PE-1-1 to PE-1-30, show stress−strain curves of similar shape. Furthermore, all curves follow quite closely the same trace up to the onset of the strong strain hardening at $e = 0.6$. That behavior seems plausible since the initial stages of the deformation process are controlled mostly by the properties of the crystalline component[12,13,18] which were practically identical in these samples. Larger differences of the stress response can be find at strains higher than 0.6. At this strain range the response of the samples PE-1-20 and PE-1-30, annealed for 20 or 30 min, respectively, was still nearly identical to that of the reference sample, while the samples annealed for a shorter time demonstrated delayed strain hardening. The PE-1-1 specimen reached the stress of 300 MPa at the strain of $e = 2.14$, while PE-1-REF and PE-1-30 developed similar stress already at $e = 2.0$. Such a different behavior of PE-1-1 as compared to PE-1-REF and PE-1-30 was, in fact, expected since PE-1-1 of the presumably reduced density of entanglements should flow more easily than entangled reference sample, and thus respond with lower stress, especially in the high strain range. On the other hand, the samples PE-1-20 and PE-1-30 were annealed long enough to restore the concentration of entanglements close to the equilibrium state (estimated reptation time, $\tau_r \sim 20$ min[22]). Therefore, these samples, having nearly identical crystalline phase and an amorphous component of very similar properties to the reference sample (including the amount, thickness of the layers, number of tie molecules and cilia, as well as the concentration of chain entanglements), should demonstrate practically identical mechanical response as the reference material not subjected to any manipulation on topology of the chain network. The experiment verified positively these anticipations.

Figure 6 presents a set of representative true stress−true strain compression curves determined for samples of PE-2. These curves show practically the same features as those obtained for PE-1. The only difference is in the behavior of chain-extended sample PE-2-CE, which appeared ductile in contrary to very brittle PE-1-CE. The PE-2-CE exhibited however the crystallinity around 93 wt %, i.e., almost 30 wt % higher than that observed in the chain-folded reference material, still not 100%, typical for PE-1-CE. The narrow amorphous layers between crystals contained the segments of the longest chains connecting adjacent chain-extended crystals, most probably highly entangled, what obstructed them to be incorporated into these crystals. These amorphous layers connected tightly to the adjacent crystalline lamellae provided notable connectivity

across crystal−amorphous layer-crystal assembly and allowed reasonable ductility of the entire material.

The elastic modulus was not very much higher than modulus of the reference sample of substantially lower crystallinity. A considerably larger difference was found in the yield stress of PE-2-CE and PE-2-REF samples. The yield point is ascribed to the activation of plastic deformation of crystalline phase by the crystallographic slip mechanisms.[40−42] The stress at yield is governed by the critical resolved shear stress of the easiest slip, which in turn is controlled by nucleation and propagation of dislocations within deforming crystal.[43,44] Since the rate of nucleation of dislocations depends on the appropriate dimension of the crystal, the critical stress for activation of any chain slip, and hence the yield stress of polymer crystals shows the strong dependence on their thickness.[44−46] Recent studies of polyethylene[47,48] demonstrated that this is only for crystal thickness below ∼40 nm. In crystals of larger thickness the yield becomes to be controlled by the rate of propagation of dislocations rather than of their nucleation, and consequently the stress at yield stabilizes at a certain (high) level for a given strain rate. It was evidenced, however, that the active deformation mechanisms of plastic deformation remain the same crystallographic slips as in samples with conventional chain-folded crystals.[48] The observed here an increase of the yield stress in sample containing chain-extended crystals (l^* ∼ 360 nm) as compared to the reference sample of much smaller chain-folded lamellae (l^* = 16 nm[18]) is in line with these findings.

After passing the yield point (45 MPa, as estimated by 2% offset) the PE-2-CE sample deformed further at relative high level of stress of around 50 MPa. At the true strain about e = 0.5 a slow increase of the true stress could be noticed, which was a mark of beginning of strain hardening. Finally, the fracture of PE-2-CE specimens was observed at the true stress of 100−170 MPa, and respective true strain of e = 1.0−1.5.

The stress−strain behavior of the samples obtained from initially disentangled melt, PE-2-t (t = 1, 3, 10, 20, 30) when compared to the behavior of the PE-2-REF reference sample demonstrated the same features as discussed previously for PE-1: complete reentangled sample PE-2-30 followed exactly the reference curve, while the sample of reduced entanglement density, PE-2-1, showed delayed strain hardening and was able to deform to higher strain than the reference material of equilibrated entanglements. The small differences of the yield and flow stresses observed among the PE-2-t specimens and PE-2-REF in the initial stage of the deformation process, which can be recognized in the inset of Figure 5, reflect a slight variation of crystallinity and lamellar thickness, as revealed by DSC measurements reported earlier in this section.

Figure 7 presents the stress reached at the true strain of e = 2.0 by samples of PE-1 and PE-2 of various thermal treatment. That arbitrary stress parameter was chosen as a simple measure of variation in the stress−strain behavior of the studied samples. The obtained plot can be used then as an illustration of the kinetic of restoration of entanglements network on annealing of initially disentangled melt. The data suggest that the sample PE-1, although initially entangled less than PE-2 (which resulted in the stress response of PE-1-1 lower than PE-2-1), was able to reach an equilibrium concentration of entanglements faster. The time of annealing necessary for reconstruction of the network can be estimated to be less than 15 min for PE-1, while around 20 min for PE-2 (such annealing seems to result in the stress−strain curve coming back to that of the reference). The difference in the kinetic of reconstruction of the network, suggested by evolution of the deformation behavior, summarized in Figure 7 can be understand easily, when taking into account different molecular weight of both polymers as well as different structure of the respective CE samples used as starting materials for this experiment (fully disentangled PE-1-CE vs PE-2-CE containing some entanglements).

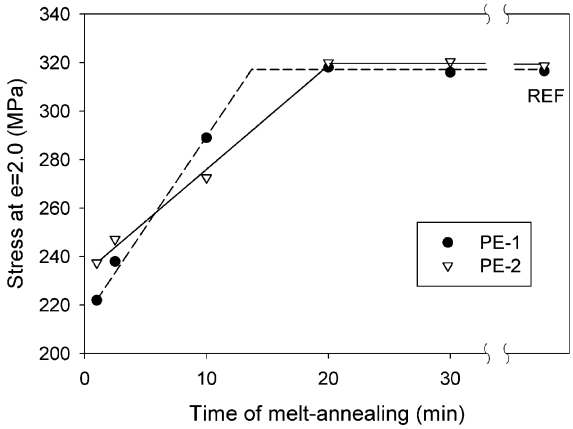

Figure 7. True stress at the true strain of e = 2.0 determined for specimens of PE-1 and PE-2 prepared by melt-annealing at 160 °C of the respective CE material, for the time indicated. Two data points at the right-hand side represent the reference samples PE-1-REF and PE-2-REF. The lines are drawn to guide the eye only.

3.4. Molecular Network Properties. The experimental true stress−true strain dependencies were compared with curves calculated on the basis of simple one-dimensional model involving plastic deformation of crystalline component and a rubber-elastic response of the molecular network, based on the hypothesis of Haward and Thackray.[3] According to this hypothesis, strain hardening originates from stretching of the molecular network of entangled chains, which can be represented in the model by the nonlinear spring element, connected in parallel with a visco-plastic dashpot representing the rate- and temperature-dependent yield and plastic and viscous flow. The 1-D and 3-D constitutive models based on Haward's hypothesis were successfully applied for several amorphous and semicrystalline polymers under various conditions of load.[3,5,49−52] Since the primary interest in this work was focused on the response of the molecular network, several simplifying assumptions were allowed here in the model formulation: the material was assumed incompressible and its initial elastic deformation could be neglected as the respective strain is small comparing to the total strain. Next, the viscoplastic response was reduced to purely plastic, represented by the plastic flow stress alone. Any dependence on the strain rate and temperature were also neglected. Moreover, any molecular relaxation phenomena within the network were not taken into account, while in the real system such processes can accommodate some of the imposed strain. Under such assumptions the true stress generated can be simply represented by the sum (dashpot and nonlinear spring in parallel)[49]

$$\sigma = Y + \sigma_R \tag{1}$$

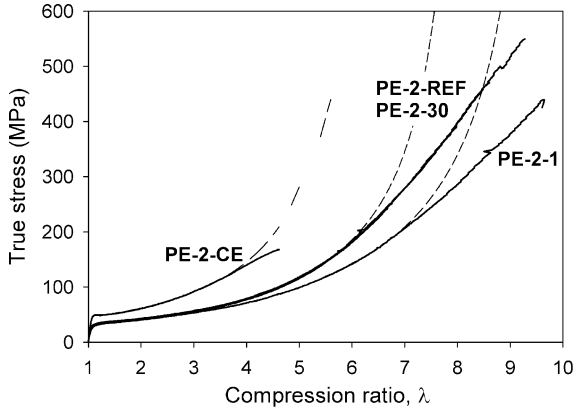

Figure 8. Experimental and fitted dependencies of true strain on compression ratio (solid and dashed lines, respectively) obtained for samples of PE-2.

where Y is the plastic flow stress and σ_R is the rubber-like stress generated by entangled molecular network. Note that the entire permanent plastic deformation of the material is achieved here in an ideal plastic process proceeding at the constant stress of Y.

The network stress σ_R was modeled using a non-Gaussian chain statistics and the eight-chain model developed by Arruda and Boyce,[53] which has been found to accurately capture the state of the stress−strain dependence of elastomers and amorphous polymers. For the plane-strain geometry the equation for the stress in the direction of loading takes the form

$$\sigma_R = \frac{G_n}{3}\sqrt{n}\,\frac{1}{\lambda_{chain}}L^{-1}\left(\frac{\lambda_{chain}}{\sqrt{n}}\right)\left(\lambda^2 - \frac{1}{\lambda^2}\right) \qquad (2)$$

where $G_n = N_e kT$ is the initial strain hardening modulus of the network (N_e denoting the effective cross-link density), n is the number of "rigid links" between cross-links (entanglements) providing limiting extensibility of a chain in the network ($\lambda_{max} = n^{1/2}$), and λ_{chain} is the stretch on each chain in that network, given by the root-mean-square of the applied strain; for plane-strain compression $\lambda_{chain} = ((\lambda^2 + 1 + 1/\lambda^2)/3)^{1/2}$, where $\lambda = CR = h_0/h$ is the compression ratio. $L^{-1}(x)$ denotes the inverse Langevin function ($L(x) = \coth(x) - 1/x$; here $x = \lambda_{chain}/n^{1/2}$), which can be accurately approximated by the Padé approximation:[49,54]

$$L^{-1}(x) = x(3 - x^2)/(1 - x^2) \qquad (3)$$

It should be noted that for large values of n eq 2 reduces to simple Gaussian equation (plane-strain):

$$\sigma_R = G_n\left(\lambda^2 - \frac{1}{\lambda^2}\right) \qquad (4)$$

Using eq 1 substituted with eqs 2 and 3, the experimental true stress-true strain curves, presented in Figures 5 and 6, were fitted in the strain range of $e = 0.1-2.0$. The parameters of the fit were a disposable plastic flow stress Y, the strain hardening modulus of the network G_n, and the number of rigid links between entanglements n. The Gaussian fits employing eqs 1 and 4 were additionally performed. Figure 8 presents exemplary results of non-Gaussian fitting obtained for samples of PE-2. The fits for PE-1 samples demonstrated the same features and quality. It can be seen that the obtained fits were reasonably good up to the compression ratio of 5−6 (true strain $e = 1.6-1.8$). For higher strains the predicted stress rises much faster than that observed experimentally. This discrepancy must be accounted primarily for simplifying assumptions done for calculations, especially that neglecting relaxation of the network.

Table 3. Molecular Network Properties of the Samples Determined by Fitting Experimental Curves

sample	E (MPa)[a]	G_n (MPa)	$N_e \times 10^{-26}$ (m^{-3})	M_e
PE-1-1	830	1.65	4.01	1290
PE-1-3		1.73	4.20	1230
PE-1-10		1.90	4.62	1120
PE-1-20		2.00	4.86	1060
PE-1-30	835	2.00	4.86	1060
PE-1-REF	820	2.00	4.86	1060
PE-2-1	770	1.91	4.64	1110
PE-2-3		1.97	4.79	1080
PE-2-10		2.04	4.96	1040
PE-2-20		2.17	5.27	
PE-2-30	760	2.17	5.27	980
PE-2-REF	710	2.17	5.27	980
PE-2-CE	1170	3.81	9.26	556
PE-melt			4.15[b]	1240[b]

[a] Determined from experimental stress−strain curves. [b] Taken from ref 37.

Another observation is that for true strain below 0.7 the experimental curves can be successfully fitted also with simple Gaussian eq 4, which means that the neo-Hookean description of the molecular network is valid in this strain range.

Table 3 summarizes the values of initial strain hardening modulus of the network, G_n, evaluated from fitting, as well as network density $N_e = G_n/kT$, and the average molecular mass between cross-links, M_e, estimated from the equation[55]

$$N_e = \frac{\rho N_A}{M_e}\left(1 - \frac{2M_e}{M_n}\right) \qquad (5)$$

where ρ is the density of amorphous phase, N_A is the Avogadro number, and M_n is the number-average molecular weight. The second term in the brackets is the Flory correction term for dangling chain ends. The calculated values of M_e are compared in Table 3 with the respective value reported for PE melt.[37]

The values obtained for G_n as well as for N_e and derived M_e are most probably quite rational—nearly the same values of G_n were obtained by both non-Gaussian and Gaussian fits; G_n shows up in the low and moderate strain portion of the curve, where all effects neglected in calculations are not critical yet. On the other hand, the values of length parameter n seem to be more uncertain, since the fits are most sensitive on this parameter in the range of high strain, where the model is much less precise due to simplifications done. The obtained parameters show a systematic variation with thermal history of the sample. In the case of both polymers the samples PE-n-30 (n = 1, 2) demonstrate the same strain hardening modulus and length parameter n as respective reference samples, while samples PE-n-1 show noticeably smaller network modulus while larger length parameter n, i.e., higher limiting network stretch ($\lambda_{max} = n^{1/2}$). The network density N_e, governing G_n, contains a contribution from chain entanglements and additionally from solid cross-links established by crystal−amorphous junctions through tie-molecules and cilia. However, the latter contribution is practically the same in samples melt-annealed for various time and in

the reference sample, since all of them were crystallized in the final step at exactly the same thermal conditions and developed very similar crystalline phase. Therefore, the observed differences of the network density can be entirely accounted for variation of the density of entanglements. Such a variation is consistent with the data of Figure 7.

The local network (entanglement) density estimated for PE-2-CE appeared surprisingly high. This can be, however, understood because those preexisting entanglements, which could not be resolved during transformation of chain-folded crystals into chain-extended form were rejected out and concentrated in the narrow layers of amorphous component, constituting about 8% of sample volume. This led to relatively high local entanglement density within amorphous layers. Nevertheless, melting of the crystalline phase results in the greatly disentangled melt—the entanglement density averaged over the entire volume is well below 1×10^{-26} m^{-3}, much less than $N_e = 4.15 \times 10^{-26}$ m^{-3}, estimated for a molten polyethylene in an equilibrium state ($M_e = 1240$[37]). If the annealing time of such melt was short (PE-2-1), only a part of entanglements was recreated, while longer annealing led to complete restoration of the entanglement network to the equilibrium level.

The results of calculations presented above supports the view that the observed variation of the deformation behavior originates from alteration of molecular network within amorphous component and is greatly influenced by the state of that network, in the entire range of the strain.

3.5. Strain Recovery Behavior. To get more insight into the influence of topology of the amorphous phase on the deformation process, the strain recovery was studied. The step-cycle experiment designed to explore the recovery behavior was described in the Experimental Section. A typical result of such experiment is shown in Figure 9. For comparison, the stress−strain curves obtained in a continuous loading regime are also shown. This figure illustrates that the curve of step-cycle test follows quite precisely the continuous curve in between successive cycles, which indicates that the deformation process is strain controlled and independent of the strain history. These features were evidenced earlier by detailed studies performed in both tension[12,13] and compression.[18]

Figure 9 shows that after deformation to a given strain the material is able to recover an appreciable fraction of that strain on unloading. That fraction consists of an instantaneous elastic part and a time-dependent inelastic part. While the former reflects the linear elastic properties of the material, the latter is related to the nonlinear reversibility of deformation of the rubbery amorphous phase. The elastic strain, associated primarily with the crystalline phase, is finite and practically constant with respect to applied strain; therefore, the dependence of strain recovery on the applied strain can supply information about the evolution of response of the amorphous phase on increasing strain.

The strain recovery through its anelastic part is a time-dependent process. The recovered component of the strain measured in the step-cycle experiment is merely a part of the strain which can be recovered over a prolonged time.[18] Only the processes characterized by relative short relaxation times can be probed in this

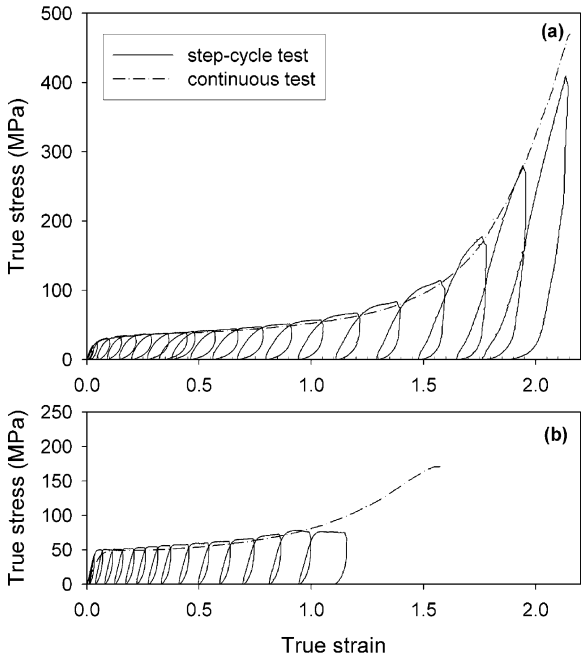

Figure 9. Exemplary true stress−true strain curves obtained in a step-cycle test: (a) PE-2-30 sample melt-annealed for 30 min after high-pressure crystallization, (b) high-pressure crystallized sample PE-2-CE. For reference the curves obtained for respective samples in a continuous loading test are plotted with dash−dotted line.

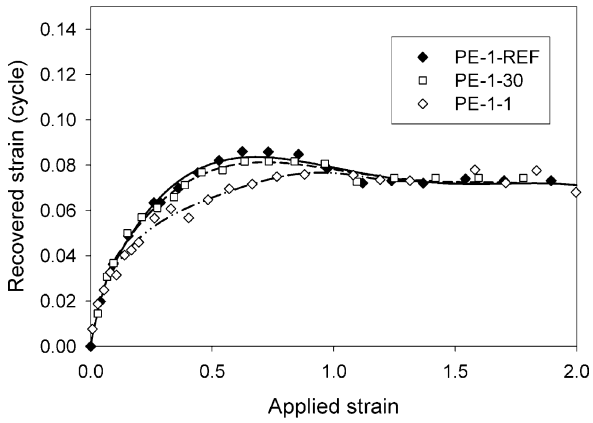

Figure 10. Dependencies of the strain recovered in cycle on the applied true strain determined for PE-1 polyethylene: black diamonds with solid line, reference sample PE-1-REF; white squares with dashed line, sample crystallized under high pressure and then melt-annealed at 160 °C by 30 min and quenched, PE-1-30; diamonds with dash-double dotted line, sample crystallized under high pressure and then melt-annealed at 160 °C by 1 min and quenched, PE-1-1.

experiment. Nevertheless, as demonstrated earlier,[12,13,18] the strain recovered on that time scale contributes significantly to the total recoverable strain and hence can be considered as an acceptable measure of the entire recovery process.

On the basis of the cycle portions of the stress−strain curve, the recovered component of the strain, e_r, as a function of the applied strain, e, was determined for samples investigated in this study. Figure 10 shows the results obtained for PE-1. The reference sample PE-1-REF exhibits the recovery curve typical for highly crystalline linear polyethylene, with a broad maximum of recovered strain component near the applied strain of 0.6, followed by a decrease and then stabilization in the plateau region in the high strain range. The

magnitude of the recovery is relative low due to high fraction of crystalline phase which, apart from the small elastic contribution, deforms irreversibly in a plastic manner. According to previous studies,[12,13,18] the following deformation sequence is responsible for the observed recovery: The initial linear increase of the recovered strain up to $e \approx 0.04$ is related mainly to the elastic response. Above this strain the elastic component is almost saturated, and plastic deformation of crystalline component sets in, but the recovered strain increases further due to increasing deformation of the network of entangled chains in sheared amorphous interlamellar layers, which have to deform cooperatively with crystals. Because of rubberlike elasticity of this network, its deformation appears partially reversible. At the strain around 0.6 the network constrained by numerous tie-molecules connecting the amorphous layer with adjacent lamellae stretches out locally nearly to its extensibility limit. Such "locking" of the deformation of amorphous component causes an increase of the stress which leads eventually to cooperative kinking (by slips) and/or partial fragmentation of crystalline lamellae at strain approaching $e = 0.6$. This results in elimination of some constraints imposed earlier on amorphous layers, which in turn allows for their further deformation. This step manifests in maximum of recovered strain component. Nevertheless, the network of entangled chains remains highly stretched and could not accommodate much more strain without pulling the chains out of entanglement knots and their permanent translations resulting in irreversible plastic flow. Such evolution of the network leads shortly to a decrease of the recoverable component of the strain. Continuation of the chain disentanglement process producing plastic flow causes stabilization of the recovered strain, with further increase of the strain in a plateau region, observed at high applied strains.

The recovery curve determined for sample PE-1-30 follows quite precisely the curve of the reference sample. This observation, along with previously reported coincidence of the stress−strain curves of these samples and network properties deduced from these curves, confirms again that these two materials have nearly identical structure of both crystalline and amorphous components. In contrary, the sample PE-1-1 of reduced entanglement density exhibits a modified curve. It does not show any maximum at $e = 0.6$. Instead, the recovered strain component increases slowly in the this range, up to $e = 1.0$, where it reaches the plateau characteristic for the entangled reference material. This demonstrates that the response of disentangled sample PE-1-1 is more plastic in character than that of reference material in the range of low and moderate true strain below 1.0; i.e., the disentangled amorphous phase responds to the applied strain with a permanent flow notably easier than the respective amorphous phase constrained by entanglements. The above result gives also a new insight into observed difference of the true stress−true strain curves of disentangled and entangled samples. The most clear difference was observed within the range of strong strain hardening, at $e > 1.0$ (cf. Figure 5), although the slope at moderate strains, reflecting the network modulus, was also slightly altered. This appears to be apparent since as demonstrated above, the differences in deformation behavior develop earlier, prior to onset of the strong strain hardening. The delayed stress response of disentangled material observed above $e = 1.0$ is then a simple consequence of that modified flow at moderate strains. Such a conclusion is in line with the already reported change of the network modulus due to the reduced number of entanglements.

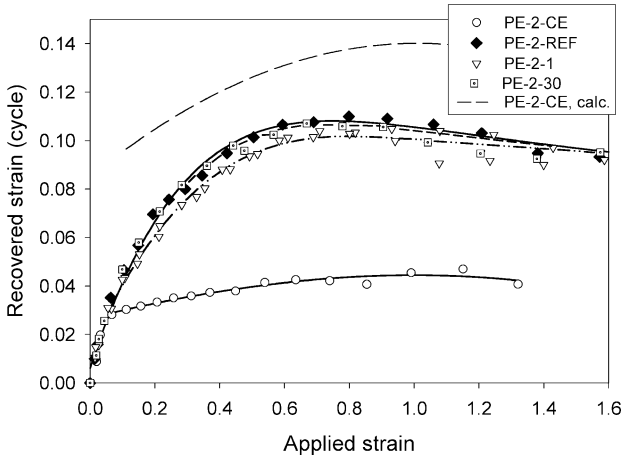

Figure 11. Dependencies of the strain recovered in cycle on the applied true strain determined for PE-2 polyethylene: black diamonds with solid line, reference sample PE-2-REF; white circles with solid line, high-pressure crystallized sample, PE−2-CE; white squares with dashed line, sample crystallized under high pressure and then melt-annealed at 160 °C by 30 min and quenched, PE-2-30; diamonds with dash-double dotted line, sample crystallized under high pressure and then melt-annealed at 160 °C by 1 min and quenched, PE-2-1. Long dashed line without symbols represents the recovery behavior of a virtual chain extended sample of assumed crystallinity $X_c = 64$ wt %, calculated from the data of PE-2-CE sample ($X_c = 93$ wt %).

A similar set of recovery curves, determined for PE-2, is presented in Figure 11. One can find here the behavior analogous to that observed for PE-1 discussed above: the reentangled sample PE-2-30 responds on applied strain identically as the reference material, while the sample of reduced entanglement density PE-2-1 demonstrates less recovery, i.e., easier flow of amorphous component in the applied strain range $e = 0.1-1.0$. On this basis, similar conclusions to those for PE-1 can be drawn also for this polymer.

Figure 11 presents additionally the recovery curve of the chain-extended sample PE-2-CE. This curve coincides with the others up to the saturation of elastic strain component. Then, it goes almost flat at the level of recovered strain of $e_r = 0.03-0.04$, up to the point of fracture. The PE-2-CE sample contain about 7 wt % of amorphous material, yet entangled more than that in the reference material (cf. Table 3). It can be expected that the strain response of the material of such topology should be a notably reversible rubberlike deformation, while the experimental curve does not seem to evidence that, at first look. However, it is only apparent, and the expected enhanced reversible behavior is, in fact, the case here. An effect of higher reversibility of deformation of amorphous layers is simply covered up due to very small fraction of the amorphous component in the material (∼7% vs ∼36% in the reference sample). As a result, the sample containing a small amount of highly reversible amorphous component shows a relatively low strain recovery. In the previous study of the recovery behavior of PE,[18] the dependence of the recovered strain component on the amount of amorphous phase was determined. On the basis of that experimental dependence, the data of recovery of PE-2-CE sample were

recalculated by setting a "virtual" crystallinity level of 64 wt %, comparable with that of the other samples in this set. Then, such a recalculated recovered strain becomes noticeably higher than that observed in the reference material of the same fraction of amorphous phase (cf. Figure 11). This confirms relatively highly reversible behavior anticipated for highly entangled topology of the amorphous phase in the PE-2-CE sample.

4. Conclusions

The experiments described in this report allowed to produce samples of semicrystalline polyethylene in which the chain topology within the amorphous component was altered by using two-stage processing including crystallization at high pressure in the first step and controlled melt-annealing followed by quenching in the second step. Samples of nearly identical crystalline component while various level of entanglements density within the amorphous component, varying from much disentangled state through equilibrium state of the entangled network up to the network of considerable increased density of entanglements were prepared and tested in plane-strain compression. Modification of the density of entanglements resulted in variation of the rubbery elastic properties of the network constituted in the amorphous component by entangled chains. The properties of this network influence markedly the response of the material to strain during the deformation process.

The reported experiments evidence that the state of the network governed by entanglements density is one of the key parameters controlling the response of semicrystalline polymer on imposed strain. Depending on the density of entanglements an amorphous component can show various amount of rubberlike recoverable deformation and permanent plastic flow. In samples of reduced concentration of entanglements the permanent plastic flow is easier than in materials of higher entanglement density and can set in quite early, at relatively low strains, becoming then a favorable deformation mechanism of the amorphous component. As a result, the strong orientation strain hardening is postponed to higher strains as compared to samples of equilibrium entanglement density. When the topology of amorphous component is modified to increase the network density that network become stiffer, with reduced ability of strain induced disentangling of chains. Consequently, there is relatively less permanent flow and the strain hardening begins earlier than in the reference material of unaltered chain topology. Such a material demonstrates additionally lower strain at break due to lowered limiting network stretch, controlled directly by the network density.

Acknowledgment. The author thanks Prof. A. Galeski and Dr. T. Kazmierczak for help in DMTA experiments and stimulating discussions. Grant 7 T08E 036 19 from the State Agency for Scientific Research of Poland is acknowledged for partial financial support. This work was also financed in part as a research project from the budget sources for science in the years 2005−2008.

References and Notes

(1) Haward, R. N. *Trans. Faraday Soc.* **1942**, *38*, 394−403.
(2) Hoff, E. A. W. *J. Appl. Chem.* **1952**, *2*, 441−448.
(3) Haward, R. N.; Thackray, G. *Proc. R. Soc. London A* **1967**, *302*, 453−472.
(4) Haward, R. N. *J. Polym. Sci., Part B: Polym. Phys.* **1994**, *33*, 1481−1494.
(5) Haward, R. N. *Macromolecules* **1993**, *26*, 5860−5869.
(6) Tervoort, T. A.; Govaert, L. E. *J. Rheol.* **2000**, *44*, 1263−1277.
(7) Strobl, G. *The Physics of Polymers. Concepts for Understanding Their Structures and Behavior*; Springer: New York, 1997.
(8) Arridge, R. G. C.; Barham, P. J.; Keller, A. *J. Polym. Sci., Polym. Phys. Ed.* **1977**, *15*, 389−401.
(9) Lemstra, P. J.; van Aerle, N. A. J. M.; Bastiaansen C. W. M. *Polym. J.* **1987**, *19*, 85−98.
(10) Bastiaansen, C. W. M.; Meijer, H. E. H.; Lemstra, P. J. *Polymer* **1990**, *31*, 1435−1439.
(11) Lemstra, P. J.; Bastiaansen, C. W. M.; Rastogi, S. In *Structure Formation in Polymeric Fibres*; Salem, D. R., Ed.; Hanser: Munich, 2000.
(12) Hiss, R.; Hobeika, S.; Lynn, C.; Strobl, G. *Macromolecules* **1999**, *32*, 4390−4403.
(13) Hobeika, S.; Men, Y.; Strobl, G. *Macromolecules* **2000**, *33*, 1827−1833.
(14) Fu, Q.; Men, Y.; Strobl, G. *Polymer* **2003**, *44*, 1927−1933.
(15) Fu, Q.; Men, Y.; Strobl, G. *Polymer* **2003**, *44*, 1941−1947.
(16) Men, Y.; Strobl, G. *J. Macromol. Sci., Phys. B* **2001**, *40*, 775−796.
(17) Al-Hussein, M.; Strobl, G. *Macromolecules* **2002**, *35*, 8515−8520.
(18) Bartczak, Z. *Polymer*, in press.
(19) Schrauwen, B. A. G.; Janssen, R. P. M.; Govaert, L. E.; Meijer, H. E. H. *Macromolecules* **2004**, *37*, 6069−6078.
(20) Smith, P.; Chanzy, H. D.; Rotzinger, B. P. *Polym. Commun.* **1985**, *26*, 258−260.
(21) Maxwell, A. S.; Unwin, A. P.; Ward, I. M. *Polymer* **1996**, *37*, 3293−3301.
(22) Psarski, M.; Piorkowska, E.; Galeski, A. *Macromolecules* **2000**, *33*, 916−932.
(23) Barham, P. J.; Sadler, D. M. *Polymer* **1991**, *32*, 393−395.
(24) Rastogi, S.; Spoelstra, A. B.; Goosens, J. G. P.; Lemstra, P. J. *Macromolecules* **1997**, *30*, 7880−7889.
(25) Wunderlich, B.; Melillo, L. *Makromol. Chem.* **1968**, *118*, 250−256.
(26) Prime, R. B.; Wunderlich, B. *J. Polym. Sci., Part A2: Polym. Phys.* **1969**, *7*, 2061−2097.
(27) Geil, P. H.; Anderson, F. R.; Wunderlich, B.; Arakawa, T. *J. Polym. Sci., Part A: Gen. Pap.* **1964**, *2*, 3703−3706.
(28) Rees, D. V.; Bassett, D. C. *J. Polym. Sci., Part A2: Polym. Phys.* **1971**, *9*, 385−406.
(29) Gruner, C. L.; Wunderlich, B.; Bopp, R. C. *J. Polym. Sci., Part A2: Polym. Phys.* **1969**, *7*, 2099−2113.
(30) Bassett, D. C.; Block, S.; Piermarini, G. J. *J. Appl. Phys.* **1974**, *45*, 4146−4150.
(31) Yasuniwa, M.; Tsubakihara, S.; Yamaguchi, M. *J. Polym. Sci., Part B: Polym. Phys.* **1997**, *35*, 535−543.
(32) Hatakeyama, T.; Hanetsuna, H.; Hashimoto, T. *J. Macromol. Sci., Phys. B* **1973**, *7*, 411−415.
(33) Kazmierczak, T.; Galeski, A. *J. Appl. Polym. Sci.* **2002**, *86*, 1337−1350.
(34) Wunderlich, B.; Czornyj, G. *Macromolecules* **1977**, *10*, 906−913.
(35) Ollley, R. H.; Basset, D. C. *Polymer* **1982**, *23*, 1707−1710.
(36) Basset, D. C.; Hodge, A. M. *Proc. R. Soc. London A* **1981**, *377*, 25−29.
(37) Pearson, D. S.; Fetters, L. J.; Graessley, W. W.; Strate, G. V.; von Meerwall, E. *Macromolecules* **1994**, *27*, 711−719.
(38) Cassagnau, P.; Montfort, J. P.; Martin. G.; Monge, P. *Rheol. Acta* **1993**, *32*, 156−167.
(39) Boyd, R. H. *Polymer* **1985**, *26*, 1123−1133.
(40) Bowden, P. B.; Young, R. *J. Mater. Sci.* **1974**, *9*, 2034−2051.
(41) Lin, L.; Argon, A. S. *J. Mater. Sci.* **1994**, *29*, 294−323.
(42) Oleinik, E. F. *J. Polym. Sci., Ser. C* **2003**, *45*, 17−117.
(43) Young, R. J. *Mater. Forum* **1988**, *11*, 210−216.
(44) Crist, B. *Polym. Commun.* **1989**, *30*, 69−71.
(45) Brooks, N. W. J.; Mukhtar, M. *Polymer* **2000**, *41*, 1475−1480.
(46) Sirotkin, R. O.; Brooks, N. M. *Polymer* **2001**, *42*, 379−3797.
(47) Kazmierczak, T.; Galeski, A. *12th Int. Conference 'Deformation Yield and Fracture of Polymers*; IOM Communication: Cambridge, 2003; pp 419−422.
(48) Kazmierczak, T.; Galeski, A.; Argon, A. S. *Polymer*, in press.
(49) Haward, R. N. *Polymer* **1999**, *40*, 5821−5832.

(50) Buckley, C. P.; Jones, D. C.; Jones, D. P. *Polymer* **1996**, *37*, 2403−3414.
(51) Boyce, M. C.; Socrate, S.; Llana, P. G. *Polymer* **2000**, *41*, 2183−2201.
(52) van Dommelen, J. A. W.; Parks, D. M.; Boyce, M. C.; Brekelmans, W. A. M.; Baaijens, F. P. T. *J. Mech. Phys. Solids* **2003**, *51*, 519−541.
(53) Arruda, E. M.; Boyce, M. C. *J. Mech. Phys. Solids* **1993**, *41*, 389−412.
(54) Cohen, A. *Rheol. Acta* **1991**, *30*, 270−273.
(55) Flory, P. J. *Principles of Polymer Chemistry*; Cornell University Press: Ithaca, NY, 1953.

MA050815Y